analytical chemistry

Article

Cite This: *Anal. Chem.* 2018, 90, 6102−6108

pubs.acs.org/ac

Cyclic-Voltammetry-Based Solid-State Gas Sensor for Methane and Other VOC Detection

Pierre-Alexandre Gross,*[†,‡] Thomas Jaramillo,[‡] and Beth Pruitt[†]

[†]Stanford Microsystems Laboratory and [‡]Jaramillo Research Group, Stanford University, Stanford, California 94305, United States

ABSTRACT: We present the fabrication, characterization, and testing of an electrochemical volatile organic compound (VOC) sensor operating in gaseous conditions at room temperature. It is designed to be microfabricated and to prove the sensing principle based on cyclic voltammetry (CV). It is composed of a working electrode (WE), a counter electrode (CE), a reference electrode (RE), and a Nafion solid-state electrolyte. Nafion is a polymer that conducts protons (H^+) generated from redox reactions from the WE to the CE. The sensor needs to be activated prior to exposure to gases, which consists of hydrating the Nafion layer to enable its ion conduction properties. During testing, we have shown that our sensor is not only capable of detecting methane, but it can also quantify its concentration in the gas flow as well as differentiate its signal from carbon monoxide (CO). These results have been confirmed by exposing the sensor to two different concentrations of methane (50% and 10% of methane diluted in N_2), as well as pure CO. Although the signal is positioned in the H_{ads} region of Pt, because of thermodynamic reasons it cannot be directly attributed to methane oxidation into CO_2. However, its consistency suggests the presence of a methane-related oxidation process that can be used for detection, identification, and quantification purposes.

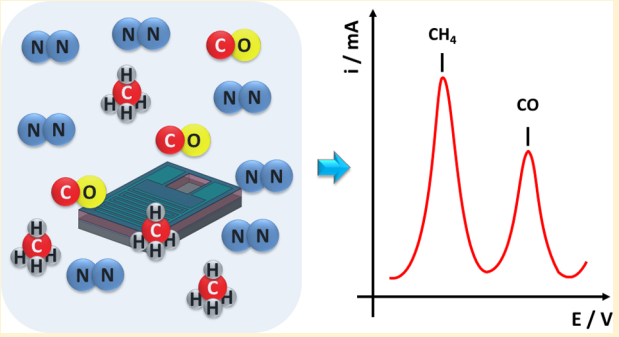

Methane (CH_4) is 25 times more effective at trapping heat in the atmosphere than CO_2, making it a dangerous contributor to the greenhouse gas effect. In addition, it is a very hazardous gas that can explode and cause severe damages. For these reasons, the detection of methane emissions is of major importance both for safety and environmental reasons. The two major sources of methane associated with human activity are agriculture (188 million tons of CH_4 per year) and fossil fuel production and usage (105 million tons of CH_4 per year).[1] According to the U.S. Department of Transportation, the distribution pipelines carrying natural gas to homes and businesses in the US suffer an average of one leak every other day. These factors create a major need for sensing technologies capable of detecting leaks and emissions. Although natural gas is a mixture of gases, methane is in the highest proportion (>80%) and is also the most volatile due to its small size and nonpolarity.

Modern methane leak detection systems are intermittent and require large pieces of equipment to be carried along pipelines. These sensors are usually loaded in the back of a car such as the Picarro Surveyor or on a plane, and are based on infrared analysis. Two types of infrared analysis are common for sensing: optical and spectroscopic.[2−4] The optical gas imaging (OGI) approach relies on gathering videos recorded in the infrared (IR) region, which are then analyzed by algorithms to identify gas leaks.[5,6] The quality of the method used to identify the leaks is determined by the maximum distance from which leaks can be detected. A major drawback of this technique is the lack of chemical identification of the detected gas stream. In the spectroscopic approach, an infrared spectrometer is used to analyze the IR absorption spectrum of the air sampled near pipelines. The spectrum exhibits typical absorption peaks corresponding to methane or other natural gas components, which are precise chemical information. This information coupled with data from a global positioning system (GPS) allows for determining the location of leaks.

Despite the fact that the infrared detection techniques are very precise, they are very costly, are intermittent, and require several people to operate them. A very promising method that addresses these issues for gas detection is the use of microsensors. They are usually inexpensive due to their fabrication using standard microfabrication tools, which makes them mass deployable. In particular, they could provide first-hand continuous monitoring of natural gas facilities or they could be deployed close to pipeline junctions were most of the leaks occur.

Attempts to microfabricate IR-based detection principles have been made, and in particular, sensor chips based on the principle of mid-infrared fiber-optic evanescent wave spectroscopy (FEWS) have been developed.[7] However, these sensors are still nontrivial to manufacture, and they depend on the development of efficient and inexpensive mid-infrared laser diodes. One of the most promising microsensors for the detection of VOCs, including methane and other hydrocarbons,

Received: January 12, 2018
Accepted: April 12, 2018
Published: April 12, 2018

DOI: 10.1021/acs.analchem.8b00184
Anal. Chem. 2018, 90, 6102−6108

are metal-oxide sensors. These sensors are usually easy to manufacture and can be integrated with electronics to produce sufficiently sensitive yet inexpensive devices. They rely on the measurement of the change in conductivity of a metal-oxide sensing layer located between two electrodes as molecules adsorb on it.[8−10] This sensing layer is usually composed of a nanostructured metal oxide such as ZnO,[11] SnO_2,[12] or TiO_2,[13] which depends on the targeted molecule. Each of these metal oxides is used because of its high affinity for a particular VOC. The main disadvantages of this type of sensors are the need to heat the sensing layer to high temperatures (300−500 °C) in order to activate it, and they are not conducive for quantifying the concentration of gases.

In the present paper, we propose that an electrochemical sensor based on CV can be used to overcome these limitations while keeping all of the advantages. These advantages are: compatibility with microfabrication techniques, cost effectiveness, and system integration capabilities. This sensing principle is based on the measurement of an oxidation or reduction current as a voltage is swept between two potential limits (E_1 and E_2) at two electrodes (WE and CE). When this voltage reaches the redox potential of a molecule adsorbed on the electrode, it gets oxidized or reduced and generates a measurable current at this applied voltage. With the help of a third electrode (the RE), the applied voltage that triggers a reaction can be associated with a particular redox reaction. A last component, the electrolyte, is necessary to complete this process. The role of the electrolyte is to conduct ionic products from the WE to the CE in order to close the electrochemical circuit. Chemical sensors based on a similar sensing principle are usually based on ytteria stabilized zirconnia (YSZ) electrolytes, which conduct oxygen ions.[14] However, these solid-state electrolytes only conduct ions at high operating temperatures (500−700 °C); that is why, in order to operate at room temperature, a polymeric electrolyte such as Nafion, which conducts protons (H^+), would be more appropriate.[15,16]

Typical redox reactions of molecules discussed in this paper are presented, along with their standard redox potential against the standard hydrogen electrode (SHE), eq 1 for the complete oxidation of methane into CO_2 and eq 2 for the oxidation of CO into CO_2.

$$CH_4 + H_2O \leftrightarrow CO_2 + 6H^+ + 6e^- \quad E^\circ = 0.17V \qquad (1)$$

$$CO + H_2O \leftrightarrow CO_2 + 2H^+ + 2e^- \quad E^\circ = 0.52V \qquad (2)$$

In a typical detection experiment using such a sensor, the CV curve is treated with a series of mathematical processes to extract the valuable information. The output of CV measurements (cyclic voltammograms) can be separated into two branches. The first one from E_1 to E_2, called the anodic branch, is where oxidation reactions are observed, and the second one from E_2 to E_1, called the cathodic branch, is where reduction reactions are observed. In the case of oxidations (cases presented in this paper), only the anodic branch contains detection information, and the cathodic branch can thus be disregarded. Also, a baseline curve, acquired under an inert atmosphere, is subtracted from the curve exhibiting the detected oxidation peaks. Ideally, this mathematical process generates a curve that resembles the one shown in Figure 1 with one peak for each molecule that has been oxidized on the surface of the electrodes. Molecules can then be identified using the position of these peaks on the potential scale. Moreover, the area under the peak can be used to determine the concentration of detected molecules by calibrating the area with a known concentration of the molecule in the gas flow.

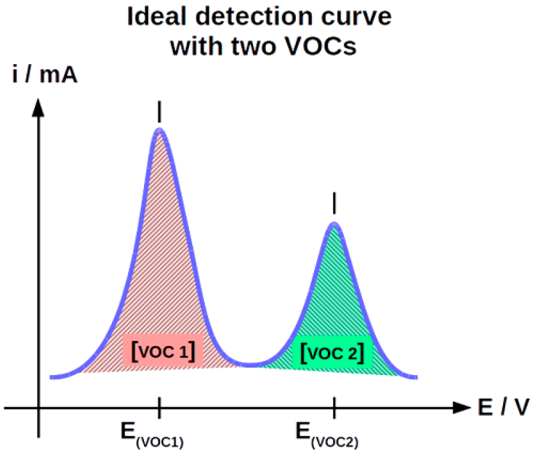

Figure 1. Electrochemical gas sensor differentiates and quantifies VOCs based on their unique oxidation potentials.

We have published some early work for the detection of CO using this principle and showed that a sensor composed simply of two Pt electrodes and a solid-state electrolyte such as Nafion is capable of detection and identification.[17,18] Pt has a strong affinity for CO, and is easy to detect using this configuration. However, methane is far less reactive. In particular, its adsorption on metallic surfaces at room temperature is very weak and is the limiting step of any electrocatalytic process where it is involved.[19] Nevertheless, this electrochemical sensing principle can in theory detect any organic molecule, as all of them can be either oxidized or reduced. We propose in this paper to use this detection principle with an updated design of the sensor for the detection, identification, and quantification of methane dissolved in N_2. This study proposes the exploration of the capabilities of CV to be used as a sensing principle; for that purpose, we have limited the environmental exposure of the sensor to N_2 in order to better confirm the origins of the observed signals. In that configuration, we have exposed the sensor to two concentrations of methane in order to observe its linear response, and we have compared the methane signal to a signal obtained during detection of CO to prove its speciation capabilities.

EXPERIMENTAL SECTION

The design and fabrication processes of this sensor was largely based on the first generation sensor. A silver layer was added between the SiO_2 substrate and the SU-8 to act as a RE. In addition, the photoresist SU-8 was used to enhance adhesion of the Nafion layer (deposited on top of SU-8) to the substrate and to limit the dehydration of this layer by retaining water.[17] In the present configuration, the sensor has all the required components (WE, CE, RE, electrolyte) to perform cyclic voltammetry on-chip. The addition of the Ag RE enables the operation of the sensor without the need of any external reference electrode in the gas phase. Potentials measured against this Ag reference will be referred to as *versus internal reference* (vs IntRef). We chose to keep the top electrodes in Pt, as it is the material with the highest electrocatalytic activity for methane oxidation.[20] Figure 2 shows an exploded view of the layer stack composing the sensor as well as the target thickness for each layer.

DOI: 10.1021/acs.analchem.8b00184
Anal. Chem. 2018, 90, 6102−6108

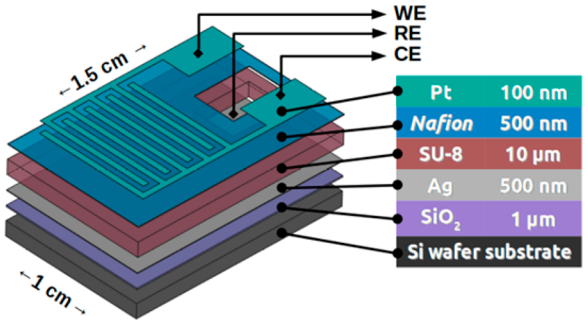

Figure 2. Sensor is composed of a reference Ag layer, an SU-8 adhesion layer, a Nafion layer, and two interdigitated Pt electrodes all on top of a Si/SiO_2 substrate. The Ag layer is made accessible from the top by cutting through the two polymers. The target thicknesses for each layer have been indicated.

Fabrication Process. A 100 mm diameter, 525 μm thick Si wafer was cleaned using a succession of baths. The baths were 9:1 H_2SO_4/H_2O_2 (piranha), followed by 5:1:1 $H_2O/H_2O_2/NH_4OH$, followed by 50:1 H_2O/HF, and finally, 5:1:1 H_2O/H_2O_2/HCl. A 1 μm thick Si dioxide (SiO_2) layer was grown on the wafers by wet oxidation at 1100 °C for 2 h 15 min. A 10 μm thick SU-8 2010 layer was spun on top of the oxide at 1500 rpm for 5 s and then at 3000 rpm for 15 s. The layer was exposed to a 119 mJ/cm^2 dose of 365 nm ultraviolet light, baked at 85 °C for 2 min to ensure hardening and drying of the SU-8, and then developed. This layer was subjected to 30 s of O_2 plasma prior to the deposition of the Nafion layer. Nafion was deposited by two consecutive drop castings of 5 mL of a Nafion D1021 water dispersion directly on the substrate sitting on a hot plate heated to 100 °C, ensuring optimal coverage of the surface. The solvent was evaporated between the castings and at the end for 10 min. This deposition process showed better results in layer homogeneity and thickness than the spin coating process used previously. To complete the layer stack shown in Figure 2, a 100 nm thick Pt layer was deposited by e-beam evaporation, at a 1 Å/s rate, through a shadow mask exhibiting the interdigitated electrode geometry. Once completed, the sensors were diced out of the wafer using a diamond tip scriber, and an electrical access to the Ag layer was cut out through the Nafion and SU-8 membranes using a razor blade. Layer thicknesses were measured at each step. Once the fabrication process was complete, the sensors were activated in a liquid environment and tested for the detection of various gases.

Characterization. All topological characterizations were made using a profilometer, and the results are presented in Table 1. The measured thicknesses presented in the table are averaged over the entire wafer and are in good accordance with the target thicknesses. The Nafion layer shows some disparity across the wafer but is thicker and more homogeneous than previously published[17] when it was deposited using spin coating.

The lifetime of the sensors has been tested by constant cycling under N_2 for 6 h. The current was stable over a period of 4 h and showed a ca. 80% diminution after 6 h of operation. This was sufficient to consider that the sensors were stable throughout the course of the testing experiments that were performed for ca. 3 h.

Table 1. Accordance of the Measured Thicknesses of the Layers Composing the Sensor with the Target Values

	thickness (nm)	
layer	target	measured
oxide−SiO_2	1000	920
reference−Ag	500	510
adhesion−SU-8	10 000	9600
electrolyte−Nafion	500	600−800
electrodes−Pt	100	110−120

RESULTS AND DISCUSSION

All experiments performed with the sensor were carried out using the test setup shown in Figure 3A, composed of a glass cell, in which the sensor was placed. Through this cell flowed a gas or a mixture of gases obtained using microflow controllers (MFCs) and a mixing chamber. All gas flows are expressed in standard cubic centimeters (sccm). The proportion of each gas is expressed as a percentage of the total gas flow of 20 sccm that exits the mixing chamber. The three electrodes (WE, CE, RE) of the sensor were connected to a Biologic SP-300 potentiostat performing CV measurements. CV curves were obtained by applying a sweeping voltage step (blue) between the WE and the CE while measuring the current at each voltage step. Once this current is plotted against the applied voltage, the CV (red) could be used to extract valuable information about the electrochemical reactions occurring on the surface of the electrodes.

Activation in Liquid. Hydration of the Nafion layer was carried out by filling the glass cell with an aqueous electrolyte of 0.1 mol/L H_2SO_4 and immersing the sensor in it. Nitrogen (N_2) was continuously bubbled in the electrolyte as the CVs were recorded between E_1 = 0.1 V vs IntRef and E_2 = 1.4 V vs IntRef. These limits were determined on larger scans spanning from −2 V vs IntRef to 2 V vs IntRef to find the position of the hydrogen evolution reaction (HER) that corresponds to 0 V on the SHE scale. Once observed close to 0.1 V vs IntRef, the upper limit was chosen in the Pt-oxide capacitive region located at slightly higher potential than their formation i.e., 1.3 to 1.5 V vs IntRef.

This experiment in liquid environment allowed both hydration and acidification of the Nafion layer.[21−23] Cycles 2, 4, and 6 of this electrochemical characterization experiment are shown in Figure 3B. One can see that cycle 2 shows no signal due to the absence of active oxidation of the Ag into Ag oxide, since no water was yet in contact with it. As the experiment continued, signals started to appear until the complete CV of Pt in acidic media was formed showing the typical peaks of hydrogen adsorption (H_{ads}) and desorption (H_{des}) and Pt-oxide formation and reduction. Once this curve was obtained, the Nafion and SU-8 membranes were considered fully hydrated; thus, the Ag layer could be oxidized and used as a reference redox potential during detection experiments. The onset of the HER was measured as 0.186 V vs IntRef in cycle 6. This value corresponds to the reference electrode shift that has to be used to normalize the observed redox signals against the SHE and allow the comparison of signals originating from different sensors. Also, this normalized potential value, against SHE, is used to identify the chemical species undergoing redox reactions on the surface of the Pt electrodes. Each chip has to be calibrated individually to determine this value, as a small variation, <5 mV, were observed. We attributed this to the slightly different chemical environment in the vicinity of the Ag

DOI: 10.1021/acs.analchem.8b00184
Anal. Chem. 2018, 90, 6102−6108

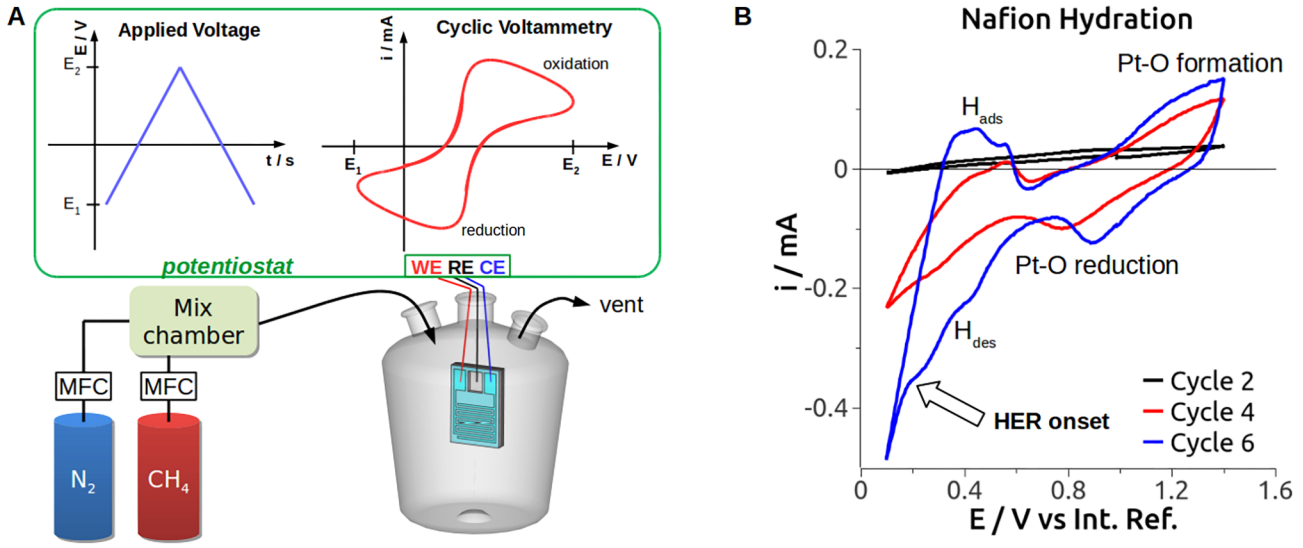

Figure 3. (A) Gas detection test setup is composed of microflow controllers (MFCs) and a mixing chamber to generated gas mixtures that flow in a glass cell where the sensor is located. The sensor is connected to a potentiostat performing cyclic voltammetry (CV). (B) Typical Pt electrochemical signals are appearing on the CV in H_2SO_4 0.1 mol/L as the Nafion layer becomes hydrated. The position of the hydrogen evolution reaction (HER) onset in cycle 6 is used to determine the reference potential shift compared to the SHE. Sweep rate is 100 mV/s.

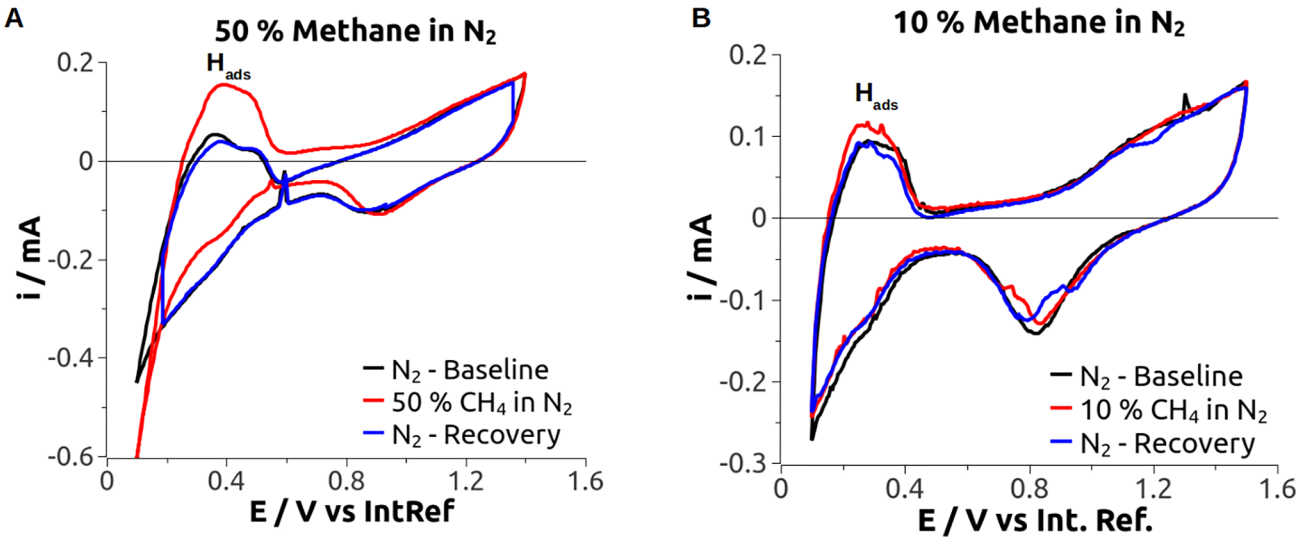

Figure 4. When methane was present in the gas flow, the H_{ads} region increases and reaches a maximum. This increase is higher for 50% methane (A), as opposed to 10% methane (B). The position of this increased signal is located at 0.38 V vs IntRef. The curve returns to its original shape when methane is turned off. Sweep rate is 100 mV/s.

layer due to small variations in the thicknesses of the SU-8 and Nafion layers.

Testing in Gas. Once the sensor has been activated in liquid, the surface of the sensor was dried out using an air stream and used for gas detection experiments. These detection experiments were carried out in the same electrochemical cell but without the liquid electrolyte as shown on Figure 3A. The gas flowed directly in the cell, at a constant flow rate of 20 sscm, after passing through the mixing chamber. All CVs were performed at constant sweep rate of a 100 mV/s. These two parameters have been chosen to make sure that the electrochemical processes involving methane are limited by its chemisorption on the Pt surface, as suggested by kinetic studies of methane oxidation on noble metal surfaces,[24,25] rather than being limited by diffusion.

Typical experiments were carried out by first acquiring a baseline curve with only N_2 flowing through the cell; then, the N_2 was adjusted proportionally as methane was added to the flow to keep the total flow constant. Two detection experiments were performed with methane: (i) 50% methane in N_2 (10 sccm methane and 10 sccm N_2) and (ii) 10% methane in N_2 (2 sccm methane and 18 sccm N_2). Finally, the methane was turned off, and pure N_2 flowed in the cell, which allowed to follow the recovery of the sensor as the curve returned back to the baseline.

Detection results are presented in Figure 4, which shows raw CVs acquired during the testing experiments described earlier, with 50% and 10% of methane in N_2. On these plots are only represented the first (baseline), the last (recovery), and the highest methane signal cycles. Intermediate cycles are not represented for clarity. The main observation that can be made

DOI: 10.1021/acs.analchem.8b00184
Anal. Chem. 2018, 90, 6102−6108

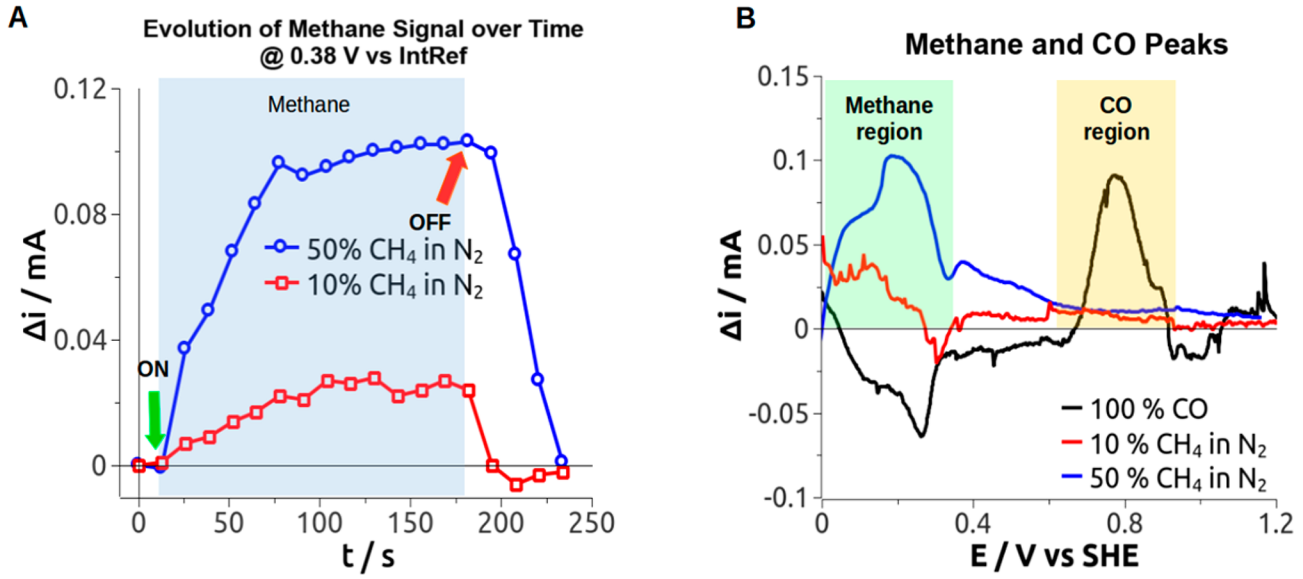

Figure 5. (A) Once the baseline is subtracted, the signals with different concentrations of methane can be compared. The amplitude of the signal is proportional to the concentration of methane in the flow, showing the quantification capabilities of the sensor. (B) The positions of the methane peaks observed in CV can be clearly identified and are well separated from a signal obtained under CO flow in similar conditions, showing the speciation capabilities of the sensor.

is the increase in current from the H_{ads} region of the Pt curve located between 0.1 and 0.6 V vs IntRef. The position of this current increase cannot be attributed to the direct oxidation of methane into CO_2, because although the standard redox potential for the oxidation of methane into CO_2 is indeed in that region (0.17 V vs SHE),[20] some overpotential is required for the oxidation to occur. Methane is known to be the least reactive hydrocarbon at room temperature, which is why its detection is so difficult.[26] Therefore, in the present conditions, observing direct electro-oxidation of methane into CO_2 is unlikely. However, observing a stable, reproducible, and proportional signal, even from indirect electrochemical processes and in a controlled atmosphere, is very encouraging for the detection of this molecule, especially using a sensor with such a simple design and fabrication process and at room temperature.

Some additional observations about these curves support the presence of an indirect electrochemical process involving methane. First, the overall shape of the curve is maintained in the region of increase, which suggests a hydrogen-related process. The particular shape of the H_{ads} region is due to the fact that the current generated by the adsorption of H on the Pt surface happens on different crystallographic planes. The precise origin of this additional H is unclear. However, it is related to the presence of methane, as it is observed only when it is present in the flow. Finally, one can also observe that when methane is present in the gas flow, the HER current increases. This feature is especially evident in Figure 4A, with a higher concentration of methane, and suggests again that H is generated during the exposure of the sensor to methane.

One hypothesis that may explain this excess of H in the system is that methane is only partially oxidized and that intermediate chemical species are generated on the surface along with adsorbed H atoms, as suggested by Psofogiannakis et al.,[24] which could be the origin of the increase in the H_{ads} current. The partial oxidation of methane is also supported by the anaerobic experimental conditions. These adsorbed H atoms may then be reduced into H_2, explaining the increase in HER current observed on the red curve. However, no clear oxidation signal, which could be attributed to methane oxidation, is observed to support this hypothesis. Yet, the fact that the overall curve is shifted upward and straightened, especially in the case of 50% methane in the flow, shows an overall increase in conductivity that could be attributed to the increase in conductivity of the Nafion layer, as the concentration of protons in it increases.

A final observation about these curves concerns the cathodic branch. The Pt−O reduction peak is shifted toward higher potentials when methane is present in the flow. This difference suggests that the methane reaction involves changes in the hydration state of the Pt oxides, which confirms the involvement of H_2O in the reaction.[27] However, this observation can also suggest that the presence of methane induces different crystalline sites to be oxidized differently, thus generating a Pt−O reduction doublet.[28] The formation of such doublet is clearly observed in the experiment with 10% methane in Figure 4B, during the recovery phase under N_2. Indeed, as shown by DFT calculations,[24] the adsorption of methane is strongly dependent on the crystalline structure and crystallographic sites present, to allow bonding with the surface Pt atoms.

The precise electrochemical analysis of the curves obtained during testing experiments is nontrivial due to several reasons. First, the absence of oxygen (O_2) in the system, as methane is mixed only with N_2. The only source of O atoms is the water molecules in the Nafion layer. Using these O atoms requires additional oxidation reactions to append simultaneously. Then, the oxidation of methane itself is a multi-step, nonlinear process, which generates several intermediates and depends on the hydration and oxidation state of the surface.[24] Finally, almost no work in similar, dry, oxygen free, gaseous conditions, at room temperature, has been reported to the best of our knowledge.

Signal Treatment. The raw CVs of Figure 4 are further transformed using a series of basic mathematical operations. The main signal for the detection of methane being observed

DOI: 10.1021/acs.analchem.8b00184
Anal. Chem. 2018, 90, 6102−6108

on the anodic branch, the cathodic branch can be disregarded and removed. Then, to isolate the part of the oxidation peak that can be attributed to the presence of methane in the flow, the baseline CV, acquired under N_2, is subtracted from each CV acquired under CH_4 flow.

In Figure 5A, the values of the current at 0.38 V vs IntRef, for each cycle of the curves from Figure 4, are plotted against time, which is determined by the 100 mV/s sweep rate. This shows the evolution of the methane signal over time, as well as the linear response of the sensor to the concentration of methane in the flow. On these curves, one can see that the signal increases as soon as methane flows in the cell and continues to increase until it reaches a steady state. The sensor shows a good response time to the presence of methane in the gas flow, ca. 13 s (the time needed to complete one full cycle), which is in good accordance with the response times of sensors with similar designs.[29]

Figure 5A shows that the increase of the signal is proportional to the concentration of methane, as it is about five times higher with 50% methane flow than with 10% flow and also that the surface does not saturate at these concentrations of methane. This proportionality shows the possibility of using the current value to quantify the concentration of methane and shows the linear response of the sensor to an increasing methane concentration. When methane is removed from the gas flow, it only takes a few cycles to go back to the baseline value, showing the good recovery time (in the order of tens of seconds to a minute) of the sensor. The signal going back to its original value shows that the surface does not get poisoned. A small overshoot is observed for the 10% methane experiment, which can be attributed to the mathematical operation that is performed to obtain this curve. Indeed, a single value has been taken as baseline and has been subtracted from all subsequent curves, but we observed that when the system is left cycling freely under N_2, CVs do not superimpose perfectly and exhibit a small variation ca. 1%. This could possibly be avoided by diminishing the sweep rate of the experiment; however, this would also diminish the current amplitude, which is undesired as it is already on the order of tens of μA. Nevertheless, the fact that the curve gets back to its original value is another advantage of cycling, as the application of higher voltages eventually oxidizes and desorbs all molecules.

In Figure 5B, the anodic branches of the cycles with the highest current value are plotted together for the two experiments under methane and for an experiment under CO. Additionally, these curves are corrected from the reference electrode shift in order to plot them against the SHE. First, the blue curve (50% methane in N_2) shows a clear peak centered at 0.2 V vs SHE that corresponds to the signal observed on Figure 4A. This peak is the main detection signal coming from the presence of methane in the gas flow. When the concentration of methane is decreased to 10%, the detection signal becomes weaker, and the signal-to-noise ratio decreased. Nevertheless, the maximum of the red curve is in the same region as the blue one, suggesting that similar electrochemical processes are happening at lower concentration.

The methane signals were compared to a signal obtained with CO (black curve) in similar conditions and processed using the same mathematical treatments. This experiment was presented in greater detail in our previous publication.[17] The peak observed on the black curve corresponds to CO oxidation into CO_2. The signal is located at 0.8 V vs SHE and is clearly separated from the signals obtained with methane. This result shows that cyclic voltammetry can differentiate molecules by their respective redox potential by producing curves with different peaks for different chemical species, as suggested in Figure 1, in the Introduction.

CONCLUSION

We have presented an updated gas sensor design that uses CV to perform electrochemical measurements. The main addition to the previously published sensor is the presence of an incorporated Ag reference electrode layer sitting underneath the SU-8 layer. The oxidation of this Ag layer during operation provides a reference potential that is used to identify the redox reactions occurring on the surface of the Pt electrodes exposed to the gas flow. Our sensor design was used to prove the capability of this sensing principle to detect methane dissolved in N_2. The results show clear and reproducible oxidation signals that were attributed to the presence of methane in the gas flow. The position of this signal for methane was compared to CO and was found to be clearly separated from it, proving the speciation capabilities of the sensor. In addition, our experiments showed that it is possible to use the current value to quantify the detected molecule in the gas flow.

We have successfully demonstrated the advantages of our microfabricated electrochemical gas sensor and its sensing principle. This principle can now be applied to more advanced designs to determine crucial specs such as detection limits, response time, recovery time, lifetime and to move towards more field-deployable devices.

Moreover, this study also showed that due to the complexity of the signal, additional environmental information would be of great help, in particular, humidity and temperature, which are known to have a significant impact on electrochemistry. This data could be obtained by either cofabricating these sensors on the same chip or through off-the-shelf sensors. By combining the environmental data to the chemical data, this system would be capable of delivering high quality detection results in continuous monitoring applications.

AUTHOR INFORMATION

Corresponding Author

*Phone: (+1) 650-285-8955; E-mail: pialgr@stanford.edu.

ORCID

Pierre-Alexandre Gross: 0000-0003-3295-5461

Thomas Jaramillo: 0000-0001-9900-0622

Author Contributions

The manuscript was written through contributions of all authors. All authors have given approval to the final version of the manuscript.

Notes

The authors declare no competing financial interest.

ACKNOWLEDGMENTS

Authors would like to thank the generous financial support of the Pacific Gas & Electric (PG&E) as well as the support of the Natural Gas Initiative (NGI) at Stanford. Additionally, authors are thankful to all staff members of the Stanford Nanofabrication Facility (SNF) for their support.

REFERENCES

(1) Global Carbon Project (GCP). http://www.globalcarbonproject.org/methanebudget/ (accessed Jun 22, 2017).

DOI: 10.1021/acs.analchem.8b00184
Anal. Chem. 2018, 90, 6102−6108

(2) Liu, H.; He, Q.; Zheng, C.; Wang, Y. *Optoelectron. Lett.* **2017**, *13*, 100−103.
(3) Michel, A. P. M.; Kapit, J.; Witinski, M. F.; Blanchard, R. *Appl. Opt.* **2017**, *56*, E23−E29.
(4) Wittstock, V.; Scholz, L.; Bierer, B.; Perez, A. O.; Wöllenstein, J.; Palzer, S. *Sens. Actuators, B* **2017**, *247*, 930−939.
(5) Ravikumar, A. P.; Wang, J.; Brandt, A. R. *Environ. Sci. Technol.* **2017**, *51*, 718−724.
(6) Burr, T.; Hengartner, N. *Sensors* **2006**, *6*, 1721−1750.
(7) Raichlin, Y.; Katzir, A. *Appl. Spectrosc.* **2008**, *62*, 55A.
(8) Liu, X.; Cheng, S.; Liu, H.; Hu, S.; Zhang, D.; Ning, H. *Sensors* **2012**, *12*, 9635−9665.
(9) Wang, T.; Huang, D.; Yang, Z.; Xu, S.; He, G.; Li, X.; Hu, N.; Yin, G.; He, D.; Zhang, L. *Nano-Micro Lett.* **2016**, *8*, 95−119.
(10) Schwarz, M. A.; Hauser, P. C. *Lab Chip* **2001**, *1*, 1.
(11) Huber, F.; Riegert, S.; Madel, M.; Thonke, K. *Sens. Actuators, B* **2017**, *239*, 358−363.
(12) Hoefer, U.; Böttner, H.; Felske, A.; Kühner, G.; Steiner, K.; Sulz, G. *Sens. Actuators, B* **1997**, *44*, 429−433.
(13) Comini, E.; Galstyan, V.; Faglia, G.; Bontempi, E.; Sberveglieri, G. *Microporous Mesoporous Mater.* **2015**, *208*, 165−170.
(14) Sekhar, P. K.; Kysar, J.; Brosha, E. L.; Kreller, C. R. *Sens. Actuators, B* **2016**, *228*, 162−167.
(15) Jordan, L. R.; Hauser, P. C.; Dawson, G. A. *Anal. Chem.* **1997**, *69*, 558−562.
(16) Jordan, L. R.; Hauser, P. C. *Anal. Chem.* **1997**, *69*, 2669−2672.
(17) Gross, P.-A.; Larsen, T.; Loizeau, F.; Jaramillo, T.; Spitzer, D.; Pruitt, B. *Micro Nano Lett.* **2016**, *11*, 798−802.
(18) Schiavon, G.; Zotti, G.; Bontempelli, G. *Anal. Chim. Acta* **1989**, *221*, 27−41.
(19) Grubb, W. T.; Michalske, C. J. *Nature* **1964**, *201*, 287−288.
(20) Eng, D.; Stoukides, M. *J. Catal.* **1991**, *130*, 306−309.
(21) Pálinkó, I.; Török, B.; Prakash, G. K. S.; Olah, G. A. *J. Mol. Struct.* **1999**, *482−483*, 29−32.
(22) Nagao, Y. *J. Phys. Chem. C* **2013**, *117*, 3294−3297.
(23) Gębicki, J.; Chachulski, B. *Sens. Lett.* **2009**, *7*, 167−176.
(24) Psofogiannakis, G.; St-Amant, A.; Ternan, M. *J. Phys. Chem. B* **2006**, *110*, 24593−24605.
(25) Wei, J.; Iglesia, E. *J. Phys. Chem. B* **2004**, *108*, 4094−4103.
(26) Otagawa, T.; Zaromb, S.; Stetter, J. R. *J. Electrochem. Soc.* **1985**, *132*, 2951−2957.
(27) Hu, C.-C.; Liu, K.-Y. *Electrochim. Acta* **2000**, *45*, 3063−3068.
(28) Tanaka, H.; Nagahara, Y.; Sugawara, S.; Shinohara, K.; Nakamura, M.; Hoshi, N. *Electrocatalysis* **2014**, *5*, 354−360.
(29) Schiavon, G.; Zotti, G.; Toniolo, R.; Bontempelli, G. *Anal. Chem.* **1995**, *67*, 318−323.

DOI: 10.1021/acs.analchem.8b00184
Anal. Chem. 2018, 90, 6102−6108